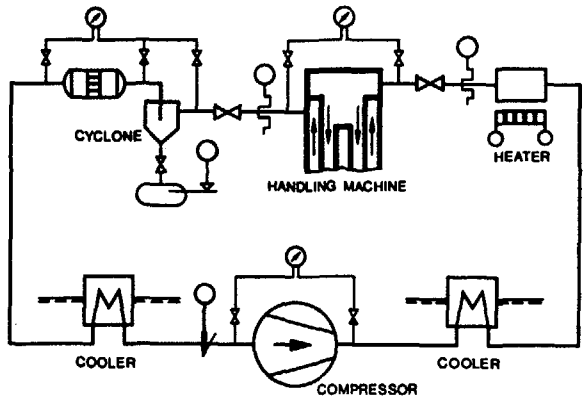

FIG. 15. HANDLING MACHINE COOLING CIRCUIT

6. Research on Aerosol Formation, Aerosol Behaviour, Aerosol Filtration Aerosol Measurement Techniques and Sodium Fires at the Laboratory for Aerosol Physics and Filter Technology at the Nuclear Research Center KARLSRUHE by S. JORDAN, W. SCHIKARSKI, W. SCHÖCK, Federal Republic of Germany

Part I

Aerosol Modelling for LMFBR Containment Systems

The behavior of aerosols in LMFBR plant systems is of great importance for a number of problems of both, normal operational and accidental kind. To mention a few:

- transport pattern of aerosols in the cover gas region (interaction with tank lid area)
- deposition of aerosols on sensitive equipment (electronics, heat changing surfaces etc.)
- aerosol transport and plate-out behavior in small and large scale sodium fires
- aerosol formation and behavior in large core accidents.

In all those events usually information is necessary on

- aerosol formation parameters
- aerosol transport pattern
- aerosol plate out processes
- countermeasures against releases.

Aerosol transport characteristics in ducts, pipes and other structures with defined streaming parameters are sufficiently well understood to apply existing theoretical approaches to real problems. In the case of closed systems (vessels) with no internal gas flow or of larger volumes with internal natural convection at present aerosol transport and behavior has not been fully understood [1].

Attemps to describe aerosol behavior in closed systems have been made in the US and in the FRG in the late 60's. Today's best computer codes available to calculate aerosol concentration time functions for closed volumes are the PARDISEKO III code [2] and the HAARM-2 code [3]. Both codes use the same integro-differential equations.

H. Jordan [4] made a comparison between HAARM-2 and PARDISEKO-III. He identified three essential differences between both codes, namely

- HAARM-2 accounts for the temperature and pressure dependence of the Knudsen number (ratio between particle radius and mean free path of carrier gas molecules) and viscosity, PARDISEKO-III does not.
- PARDISEKO-III includes two shape factors (κ and f), HAARM-2 includes the apparent reduced density of a porous particle only.
- HAARM-2 employs the theoretical solution for the collision efficiency of a spherical particle in viscous motion. PARDISEKO-III takes the collision efficiency as an input constant.
- HAARM-2 assumes the particle size to be lognormally distributed for the whole period of time under consideration allowing very short computation times. PARDISEKO-III makes no restrictions on the particle size distribution at the expense of long computation times.

The evaluation of the advantages and disadvantages of these and other features of the existing codes is important and should be done in the near future since, in particular in long term (real time) calculations, large discrepancies between result and reality might exist.

Both codes have been used for extension calculations on aerosol behavior in HCDA of LMFBR's. Here an instantaneous aerosol source is formed decaying in a closed system depending on essentially four aerosol processes, namely

- coagulation
- sedimentation
- thermophoresis
- diffusion.

These processes have been identified in our TUNA program [5] (test stand see Fig. 1) which was evaluated and compared with PARDISEKO-III [6], [7].

The agreement between the TUNA experiments, carried out with UO_2 aerosols in nitrogen, and the PARDISEKO theory was satisfactory if some from standpoint of aerosol physics reasonable assumptions on aerosol form factors are made (see Fig. 2). HAARM-2 was also applied to TUNA experimental program results [4] showing reasonable agreement with PARDISEKO-III (see Dif. 3). However, these cases represent from standpoint of aerosol physics and aerosol chemistry relatively simple aerodisperse systems.

A final test whether the theoretical assumptions made in a code for aerosol modelling are correct and lead to a description of the real accidental aerosol system with sufficient accuracy can be made only be comparison with experiments. In the frame of the FAUNA program, starting early 1977 at Karlsruhe, a larger vessel (about 200 m^3) will be available to make the necessary experiments to answer the problem. Preliminary calculations applying the PARDISEKO-III code to the sodium burning experiments in the CEN Cadarache (Cassandre program) have been carried out. One typical result is given in Fig. 4 where the sodiumoxide aerosol concentration time function is compared with a PARDISEKO-III calculation [8]. The experiment was performed in the 400 m^3 containment facilitiy at Cadarache employing the burning of 40 kg of sodium. Here, of course, other form factors than for UO_2 aerosols should apply which are given in Fig. 4. It is important to note that the time dependent source as experimentally measured was introduced into PARDISEKO-III code. It is not fully understood whether the typical result of PARDISEKO-III curve being always by some factor above the experimental curves relates to the form factors assumed ($f = 1.0$ and $\kappa = 1.0$) or to the neglection of gravitational coagulation which was not taken into account in these calculations. Since the first comparisons between PARDISEKO-III calculations with time dependent aerosol sources in large volumes [8] revealed differences more than a small factor much more work has to be done on aerosol modelling.

Part II

Aerosol Size Spectrometry by Laser Light Scattering

1. General properties of laser spectrometers

For long times the scattering of light has been a well known technique for sizing of aerosol particles. The main advantages of this method are:

- Particles are sized in the airborne state without changing their properties.
- The measurement is continuous.
- The measured values are displayed instantaneously.

These properties of light scattering aerosol spectrometers make them extremely valuable for measuring time dependent aerosol systems and instable particles, as e.g. liquid droplets.

However, this powerful technique has not been applied widely because of certain restrictions that were related to the use of incandescent light sources used for illuminating the aerosol.

The important progress was achieved with lasers as primary light sources in optical spectrometers. The high intensity and the extreme focussing properties of laser light lead to the possibility of forming adequately small sensing volumes which are necessary for measuring aerosols with high particle concentration.

Different developments in the field of laser aerosol spectrometry have been done in our laboratory. In the following sections brief reports will be given on resolution and sensitivity limits, on a method of auto-calibration and on a recent development of an in situ spectrometer for water droplet sizing.

2. Sensitivity limits of optical particle spectrometers

Empirical sensitivity limits of laser aerosol size spectrometers are in the range from 0.07 to 0.4 µm depending on input laser light intensity and on the construction of the detecting system for the scattered light pulses. Since the limits depend on careful design of the optical system and on avoiding parasite stray light, considerable efforts have been done to improve the sensitivity of spectrometers.

It is, however, possible to save unnecessary time and work for experimental development by calculating the performance data of an optical scattering system in advance. Details are given elsewhere [9], the results are the following.

Using the Mie theory for calculating the scattered light from a particle of radius r and integrating over the viewing aperture, the total detected energy is given by

$$E = P_o \cdot Q \cdot t$$

where P_o is the input light intensity and t the time of illumination of a particle. Q is a specific scattering cross section which is a function of the particular optical setup and of the optical particle properties. These being constant for a specific problem Q(r) is a function of the particle radius only. Moreover, Q(r) can be calculated absolutely and the validity of the results has been proven by experiments as will be shown in the next section.

At the moment we will consider the sensitivity limit only.

Taking into account that one photon is the smallest energy amount detectable by a photomultiplier, the sensitivity limit follows from the above equation through E_{min} = 1 photon. Considering further that the size resolution of a single photon is arbitrarily bad, one can immediately define a sensitivity limit for every postulated resolution by increasing the number of photons to a sufficiently high value.

This method does not consider the effects of background stray light because by careful design of the spectrometer and by proper selection of lasers and photomultipliers it is possible to reduce the background to such low levels that single photons scattered by the aerosol particles can be measured.

Fig. 5 shows a measurement of a droplet size distribution. The data a) suggest a log-normal size distribution which is cut off at low values. After fitting the data to a truncated log-normal function curve b) exhibits a cut off value of 0.185 µm which agrees very well with a calculated one photon limit of 0.18 µm for the spectrometer which was used for the measurement.

3. The auto-calibration method

Calculated calibration functions Q(r) of optical aerosol size spectrometers are exact as long as the optical properties of the measured particles are exactly known. This has been demonstrated using water droplets which indeed are spheres with a well known refractive index [9].

Fig. 6 shows a typical calibration function of a forward scattering spectrometer using a He-Ne laser. The oszillations of this function will produce peaks in the measured pulse height spectra of any aerosol, that is polydisperse enough to extend over one or more of the oszillations.

Fig. 7 shows an example. The solid line is the calculated pulse height spectrum using a very broad droplet size spectrum as input and the function in Fig. 6 as a transformation function. The dotted line represents measured data of a polydisperse water droplet aerosol. It is obvious that all the major peaks of the curves are retrieved. These peaks are correlated to a well known particle size.

The calibration of the spectrometer is then obtained simultaneously from the measured data. A separate experimental calibration is no more necessary. This auto-calibration method is very valuable in cases where amplification factors of a spectrometer must be changed many times. It is not necessary to spend time for recording these factors and for controlling the light input power for every single measurement, because all this information is implicitly stored in the measured pulse height spectra.

The data in Fig. 5 are obtained using this method. It can be seen that the counts in the large intervals of oszillations of the calibration function must be counted into one channel. The slight deviations of the data from the straight line are due to the limited size resolution of the apparatus.

The auto-calibration method has been applied in many experiments in our laboratory, e.g. for measuring of the size spectra of different nebulizers which are used as test aerosol generators [10].

4. In situ size spectrometry of water aerosol

A measuring problem that occured resently in one of our reactor safety programs is the measurement of the sizes of water droplets in a supersaturated steam atmosphere at elevated temperatures.

The steam droplet aerosol system is highly sensitive to changes in temperature and pressure. It is not possible to use spectrometers which draw samples from the system because the size spectra will be modified by the necessary pressure difference.

The in situ light scattering is the only suitable method that can be used to size the droplets without affecting their properties. This method has been applied for droplet sizing in cooling towers already [11]. It has, however, not been reported with lasers as light sources. In our case the high concentration of the droplets can be handled only with the very small sensing volumes that may be formed with laser light illumination.

Fig. 8 shows the scheme of the optics of the spectrometer [12]. Illumination and observation optics are constructed in parallel in order to form a probe

head which can be inserted through the wall of the vessel or tube that contains the aerosol. The laser and the photodetector are situated outside under suitable conditions. The deflected illuminating beam and the observation cone intersect at 90° and form a sensing volume of 10^{-5} ... 10^{-6} cm^3. The permissible droplet concentrations are then 10^4 ... 10^5 cm^{-3}.

At present a low power He-Cd laser is used. The wavelength of 441 nm permits efficient filtering of background light and high conversion efficiency of the photomultiplier.

Due to the optical boundaries of the sensing volume corrections have to be made for droplets that are illuminated incompletely at the borders of the sensing volume. The ratio of errouеous light pulses increases with decreasing sensing volume.

Though it is principally possible to correct the measured data for border effects, the necessary procedure is rather time consuming. So the setup of the spectrometer should be optimized for every special case, in order to keep the errors adequately low. As a rough measure the size of the sensing volume should be 100 times the size of the droplet for 10 % errouеous light pulses.

The calibration function Q(r) is shown in Fig. 9. The two extreme polarization angles can be chosen by rotating the laser around its optical axis. The dotted curves are exactly calculated Mie functions showing the typical oszillations while the solid lines represent the averaged values due to the effects of boundary errors.

The calculated sensitivity limit for a single photon event is $Q(r)=10^{-12}$ cm^2 corresponding to r=0.2 µm. Because of the steep ascent of the Q-functions up to approximately 2 µm not the total size range can be covered with a single amplification value. In most cases the size range will be set from 1 µm upward, as the droplets to be measured have diameters in this range.

Preliminary tests of the performance of this spectrometer showed the validity of the above mentioned specifications and that the instrument is operable under the conditions of a hot supersaturated atmosphere. The measurements in the test vessel will start in 1977.

Part III
Facilities and Experimental Results

For the analysis of reactor accidents the release of radioactive substances is most important. At the sodium cooled reactor most of the fission products and fuel nuclides - except noble gases - will be released in form of aerosols. Informations on the emission rates and behavior of aerosols in closed systems are therefore most important.

The formation of nuclear aerosols in case of an accident depends on the accident itself. Assuming a Bethe-Tait accident - the up to now assumed most severe hypothetical accident - one has to distingish for the SNR three kinds of aerosol sources with different composition and behavior.

1) Primary released aerosols by excursion: This are mostly Plutonium aerosols.
2) Sodium fire aerosols: The unavoidable rest oxygen of about 0.5 % in the inner containment causes a sodium-oxygen reaction. Sodiumoxid aerosols are released and may take along fission products and fuel particles.
3) Sodium pool aerosols: After a HCDA hot or boiling sodium may cover the molten fuel in a core catcher. Considerable quantities of sodium may evaporate and build condensation aerosols.These aerosols may be mixed with fission products and fuel particles.

The behavior of these three kinds of aerosols is investigated by experimental and theoretical simulation.

The behavior of primary nuclear aerosols (UO_2) was investigated in the 2 m^3 volume TUNA test facility. A diagram of the test facility is shown in Fig. 1 UO_2 aerosols were produced by the exploding wire technique in nitrogen atmosphere and the time function of aerosol concentration measured under different conditions (e.g. temperature gradients).

The long-term behavior of particle concentration has to be discriminated in three time spans. At first the concentration of particles is decreasing very fast caused by coagulation. In the second time span no special aerosol process is dominant. After two days in the third time span the concentration is decreasing exponential (sedimentation and diffusion to the walls).

Four essential aerosol processes were identified to be responsible for aerosol behavior, namely coagulation, sedimentation, diffusion and thermophoresis.

The experimental results of these experiments were already discussed in detail in part I of this paper in terms of comparison with calculations from PARDISEKO code. The necessity to introduce shape factors into the PARDISEKO theory was found.

Experiments on sodium fires and on the release of fission products from sodium pools were performed in the test facility NABRAUS (Fig. 10). This vessel of about 4 m^3 volume can be evacuated so that any desired atmosphere can be simulated. Up to 10 kg of sodium can be brought into a 1 m^2 fire pan via a glove-box. Burning rates and aerosol formation rates were found to be between 2 and 20 kg $Na/m^2 \cdot h$ at 1 respectively 21 % oxygen content [13].

The measured aerosol formation rates are compiled in Fig. 11.

Time functions of aerosol mass concentration were measured (Fig. 12).

The aerosol mass concentration over the sodium pool increased in all tests at a relatively fast rate and attained aerosol concentrations between 3 and 20 g/m^3, subsequently, aerosol concentration decreased slowly to concentrations around 0.1 g/m^3. Mass concentrations of several grams per cubicmeter were attained also at oxygen concentrations smaller than 1 ppm.

These results are important for the lay-out of filter systems.

For a second series of experiments a filter loop was added to the test rig and different types of filters were investigated concerning their behavior by loading with sodiumoxide aerosols. High efficiency sand bed filters were developed and optimized concerning load capacity and efficiency (see session IV).

The release rates of fission products from sodium pools into an atmosphere of different oxygen content was investigated in a third series of experiments.

The Cesium content in the aerosol shows a development similar to the mass concentration with the maximum Cesium concentration in the aerosol generally attained before attainment of the maximum value of the airborne sodium concentration. A multiple of the initial Cesium concentration in the pool was measured in the aerosol.

Fig. 13 shows some experimental results. For different oxygen concentrations the maximum sodium and sodiumoxide concentration, the maximum Cesium content measured in the aerosol and the Cesium content of the sodium pool before and after the test have been indicated. The results of measurements show that for a low oxygen concentration a maximum enrichment of Cesium is obtained in the aerosol. The aerosol may contain more than ten times the amount of Cesium present in the sodium pool. The Cesium content of the aerosol falls with increasing sodiumoxide aerosols production caused by an increase of the oxygen content in the atmosphere.

It can be concluded from the tests that sodium and Cesium evaporate independent of each other and that this process is governed exclusively by the temperature and vapor pressure, respectively. Due to its higher vapor pressure as compared to sodium, the aerosol gets enriched in Cesium so that gradually the Cesium content in the pool is substantially reduced. This fact is reflected in the Cesium analysis of reaction residues present in the pan after the fire (last column in Fig. 13).

Balance calculations yield for a sodium pool with a Cesium content of 100 ppm at 500-700°C a Cs evaporation rate of 5 g $Cs/m^2 \cdot h$. According to the experimental results this evaporation rate seems to be proportional to the Cesium concentration in sodium: for 500 ppm and at identical temperatures a rate of 25 g $Cs/m^2 \cdot h$ was measured [14].

The Strontium content of aerosols in another series of burning experiments was very low and quite near to the detection limit of analyzing technique. Aerosol mass concentration had a development similar to mass concentration at Cesium experiments. The Strontium content of aerosols was measured three orders of magnitude lower than pool concentration.

The release of Uranium from a hot or boiling contaminated sodium pool is investigated in the NALA test facility (Fig. 14).

At these laboratory scale experiments different quantities of Uranium dioxide powder (mean particle diameter 20 micron) were suspended in about 100 grams of sodium and heated up to 500 to 900 degree centigrade. The evaporated sodium and fuel was either transported by a gas stream of Argon or by diffusion through a heated (200°C) pipe in two cold-traps cooled with liquid nitrogen. At the end of the open loop was a filter. The gas stream was measured by a gas-meter.

The Uranium content of aerosol samples respectively the Uranium content of sodium in the cold traps was determined by fluorometric technique. By this technique it was possible to measure an Uranium content as low as 10 ng.

The concentration of fuel in each sample is compared with the concentration in the initial hot sodium pool and discussed in terms of decontamination factors DF which are the ratios of the fuel concentration in pool to the released fuel concentration in sodium aerosol.

Experimental results are placed together in Fig. 15. All experiments were performed with 100 gram of sodium and either 1 or 10 gram of Uranium dioxide suspended in sodium.

Decontamination factors were found nearly reproducable to 1500 $\pm$ 500 at sodium boiling conditions. No significant change of decontamination factor was found between the destillation experiments and those forced by Argon gas flow. The concentration of Uraniumoxide in sodium has no strong effect on decontamination factor.

In the range of error no significant temperature dependence of Uranium releases from sodium pool was found. This points to a evaporating compound boiling at much higher temperatures than sodium. Sodium uranate Na_3UO_4 might be responsible for Uranium release from contaminated pools [15].

From the experimental results it is possible to get a reference to the vaporization rate of sodium. The evaporation rate of sodium was found to be about 85 kg $Na/m^2 \cdot h$ at 900°C and about 300 g $Na/m^2 \cdot h$ at 500°C.

Large scale sodium fires and the behavior of nuclear aerosols including mixed aerosols in large volumes will be investigated in a 220 m^3 stainless steel vessel FAUNA now under construction. The vessel can be evacuated so that any desired atmosphere can be simulated. Design pressure is 4 bar. The maximum sodium mass which can be handled in FAUNA is 1000 kg.

The performance of the reventing-blowers of the German LMFBR prototype reactor SNR-300 in presence of sodiumoxide aerosols is tested in the REGINA facility. The SNR-300 reventing system is mocked up in scale 1:1. Deposition of sodiumoxide in the system and material corrosion of important components is investigated.

Part IV

Filtration of Sodiumoxide Aerosols by Multilayer Sand Bed Filters

Up to now,nuclear installations with a chance of sodium fires have been equipped with conventional fiber-glass filters. These filters have high retention efficiencies for chemically inert aerosols but do not resist aggressive sodiumoxide aerosols [16]. Sand bed filters have therefore been developed and tested for use in the exventing-system of Liquid Metal Fast Breeder. Filtration of aerosols by sand bed filters is well known although no previous attempts to optimize these filters on efficiency and loading capacity have been reported.

The experiments were carried out in a closed gas-loop shown in Fig.16 . Sodiumoxide aerosols were produced by burning 5 kg of Na in a pan of 1 m^2 area at the bottom of a chimney. The Na_2O_2 aerosol formation rate was about 20 kg $Na/m^2 \cdot h$. The maximum aerosol concentration in the test loop was 40 g/m^3.

The sand bed filter experiments entailed the construction and building of a special housing apparatus consisting of 5 mm steel sheet. The housing was gas-tight and could take up about 2 m^3 of sand. The gas flow was directed from above to below. At the bottom of the housing specially formed steel sheets were installed to provide a good gas flow. Above these steel sheet a supported sand layer of about 10-20 cm thickness was arranged followed by layers of fine graded sand. The first layer from above was usually coarse grained sand. Except for these two layers the sand was packed in such a way that the porosity ε decreased with bed depth.

In the first series of experiments the pressure drop Δp at different air flow rates was determined for a simple arrangement of sand layers. High collection efficiencies and good loading capacities were achieved for low flow rates of 400 l/min corresponding to air velocities of 0.9 cm/sec whereas at high air flow rates of 2000 l/min (4.5 cm/sec) good collection efficiencies but moderate load was measured (Fig. 17). At medium range flow rates good filtering conditions were not achieved for this sand arrangement.

It is very interesting to follow the increase of pressure drop with loading capacity at different flow velocities. For low velocities the pressure does not increase substantially up to a load of 300 g/m^2. For higher velocities the pressure increases rapidly.

Fig. 18 shows a representative selection of our experiments with different sand layers, where the different sand layers have been optimized with respect to filter efficiency and loading capacity.

It was found to be impossible [17] to get high loading capacities together with low penetrations over the whole range of flow velocity with one packing of sand layers.

Therefore a "permeable" packing (I) of sand layers for flow velocities of 2-5 cm/sec (900-2300 l/min) and a more dense one (II), by adding a thin layer of very fine graded sand, for velocities 0-2 cm/sec (0-900 l/min) was used.

From Fig. 18 it can be seen that filter efficiencies were achieved better than Hepa standard except for one experiment performed at a flow velocity of 1000 l/min for packing one. This is just the critical region between diffusional deposition inertial impaction.

Fig. 18 moreover shows that the loading capacity varies between 400 and 600 g/m^2 filtercross-section compared with a loading capacity of about 50 g/m^2 for fiber-glass filters. It may be emphasized in this connection that the loading capacity was mainly limited by the maximum pressure drop of 800 mm WG allowed for this filter arrangement.

The quality of a sand bed filter is mainly determined by the filtration processes impaction, diffusion and sedimentation. A simple penetration model for multilayer sand bed filters was developed to explain experimental results [18].

From the fact that the pressure drop Δp rises linearly with flow velocity one can conclude that the Hagen-Poiseuille law can be applied to explain the clogging of sand bed filters. It seems reasonable that the filter cake is mainly responsible for the pressure rise across the filter. One of results of this theory is shown in Fig. 19.

For three distinguished filter layers (1a, 2b, 2c) the penetration of the layers and then the penetration of the whole filter P_{tot} have been calculated. Since the deposition of the larger particles mainly takes place within the filter cake, for the upper layer (1a) a particle diameter of $\bar{d}_{pa} = 1.4$ µm has been taken. For the other layers the particle diameter of $\bar{d}_{pa} = 0.15$ µm has been used for the calculation. The experimental values scatter around the curve P_{tot}. This is a confirmation that already simple physical assumptions give a good proof for the epxeriments.

References

[1] W. Schikarski, On the State of the Art in Aerosol Modelling for LMFBR Safety Analysis, International Meeting on Fast Reactor Safety and Related Physics, Chicago, 5.-8.10.1976.

[2] H. Jordan, C. Sack, PARDISEKO-III, A Computer Code for Determining the Behavior of Contained Nuclear Aerosols, KFK 2151 (Mai 1975)

[3] L.D. Reed, I.A. Gieseke, HAARM-2 Users Manual, BMI-X-665 (1975)

[4] H. Jordan, A Comparison of HAARM-2 and PARDISEKO-III, BMI-X-667 (1975)

[5] W. Schikarski, The Karlsruhe Research Program on Nuclear Aerosols and its Relation to the Hazard of Fast Sodium Reactors, KFK 798 (July 1968)

[6] H. Jordan, W. Schikarski, H. Wild, Nukleare Aerosole in geschlossenen Systemen, KFK 1989 (Oktober 1974)

[7] W. Schikarski, The Aerosol Behavior in LMFBR accidents: Results of TUNA Experimental Program and Comparisons with PARDISEKO-Code, 14th ERDA Air Cleaning Conference, 2.-4.8.1976, Sun Valley, Idaho

[8] H. Bunz, J. Fermandjian, Interprétation des Essais CASSANDRE au moyen du Code de Calcul PARDISEKO-III, Rapport SETSSR No. 52, evolution des aerosols sodes dans une enceinte confinée (Nov, 1976)

[9] W. Schöck, Meßbereichsgrenzen und Auflösungsvermögen bei optischen Partikelgrößenspektrometern, Proceedings of "Kolloquium Aerosolmeßtechnik", IENT/RWTH, March 4,1975, Aachen, Germany

[10] W. Schöck, Messungen der Tröpfchengrößenspektren von Inhalationsverneblern, Proceedings of the First International Congress on Aerosols in Medicine, September 19-21, 1973, Baden/Vienna, Austria

[11] G. Dibelius, A. Ederhof, Fortschr. Ber. VDI-Z, Ser. 15, No. 5, pp 28-36

[12] W. Schöck, Messung von Tröpfchengrößenspektren in übersättigter Wasserdampfatmosphäre mit einem Laser-Streulichtspektrometer, Proceedings of the annual congress of the Association for Aerosol Research 1976, November 3-6, 1976, Bad Soden/Ts, Germany

[13] L. Böhm, S. Jordan, Aerosolerzeugung und Filterverhalten bei Natriumbränden, KFK 2202, 1975

[14] S. Jordan, Release of Fission Products from Contaminated Sodium Fires, International Meeting on Fast Reactor Safety and Related Physics, Chicago, 5.-8.10.1976

[15] S. Jordan, Y. Ozawa, Fuel Particle and Fission Product Release from LMFBR-Core Catcher, International Meeting on Fast Reactor Safety and Related Physics, Chicago, 5.-8.10.1976

[16] L. Böhm, S. Jordan, W. Schikarski, Experiments of Filtration of Sodium-Aerosols by Sand-Bed-Filters, Conference on Fast Reactor Safety, Beverly Hills, CA., 1974

[17] L. Böhm, S. Jordan, W. Schikarski, The Off-gas System of the SNR-300, 13th AEC Air Cleaning Conference, San Francisco, 1974

[18] L. Böhm, S. Jordan, On the Filtration of Sodiumoxide Aerosols by Multilayer Sand Bed Filters, Journal Aerosol Sci., Vol. 7, pp 311-318, 1976

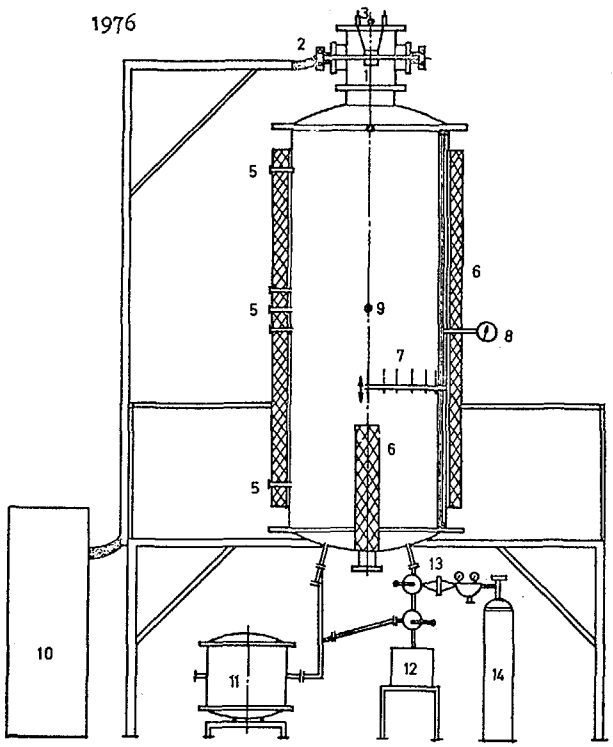

FIG. 1

TUNA, schematic

1 aerosol chamber
2 coaxial cable
3 preheater electrical penetration
4 TUNA main vessel
5 aerosol measuring ports
6 gas heater (internal, external)
7 thermocouple rig
8 manometer
9 pressure transducer
10 power supply and condenser bank
11 off-gas filter
12 pump
13 inlet filter
14 gas supply

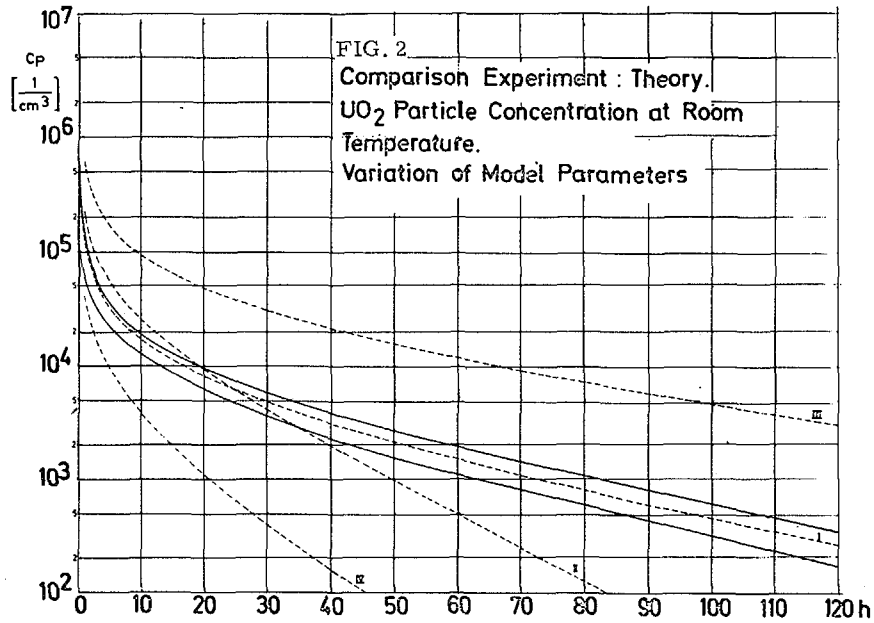

FIG. 2
Comparison Experiment : Theory.
UO_2 Particle Concentration at Room Temperature.
Variation of Model Parameters

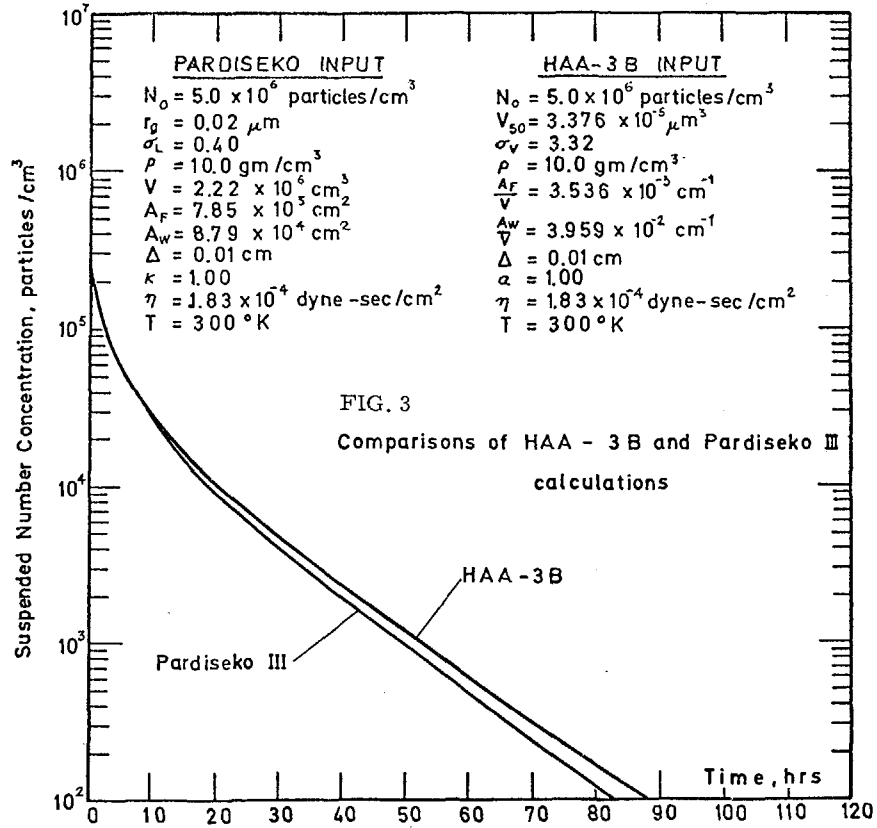

FIG. 3
Comparisons of HAA - 3B and Pardiseko III calculations

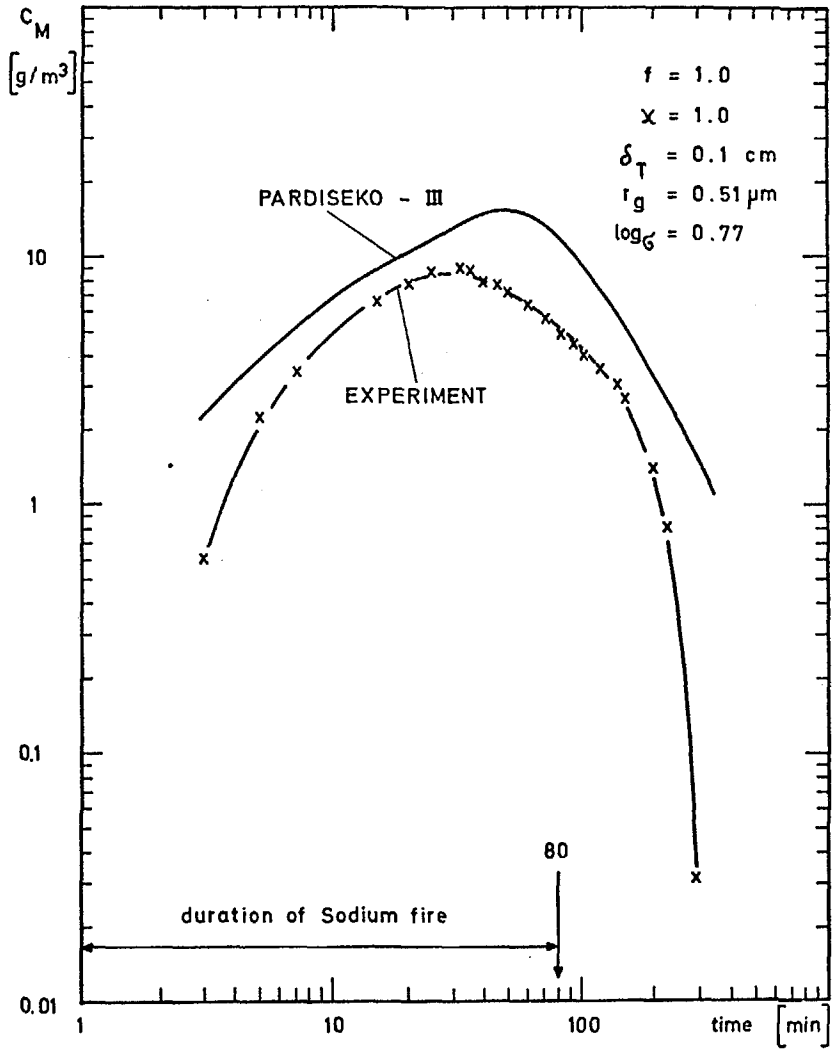

FIG. 4. Comparison of Experiment Cassandra 3 (see[5]) with PARDISEKO - III

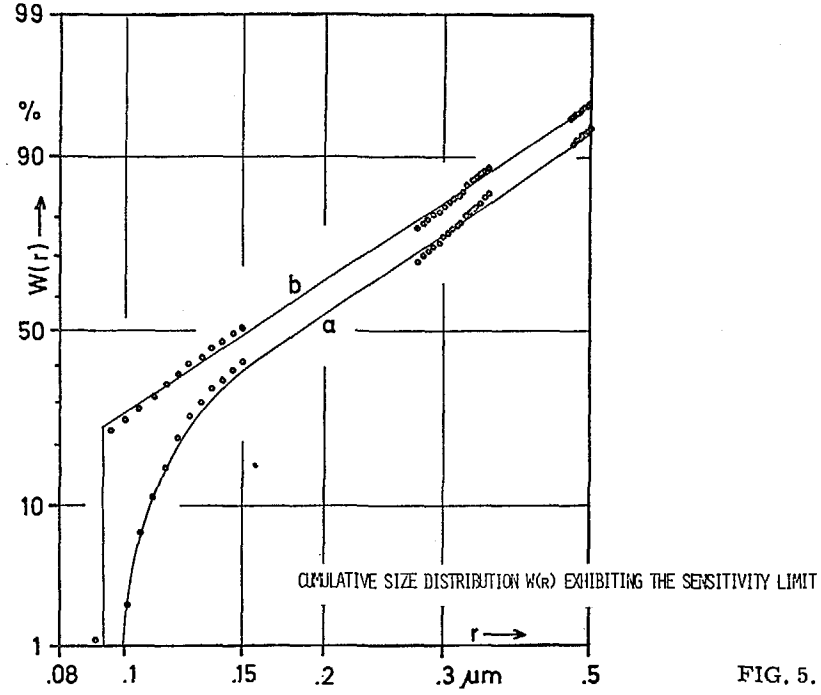

FIG. 5.

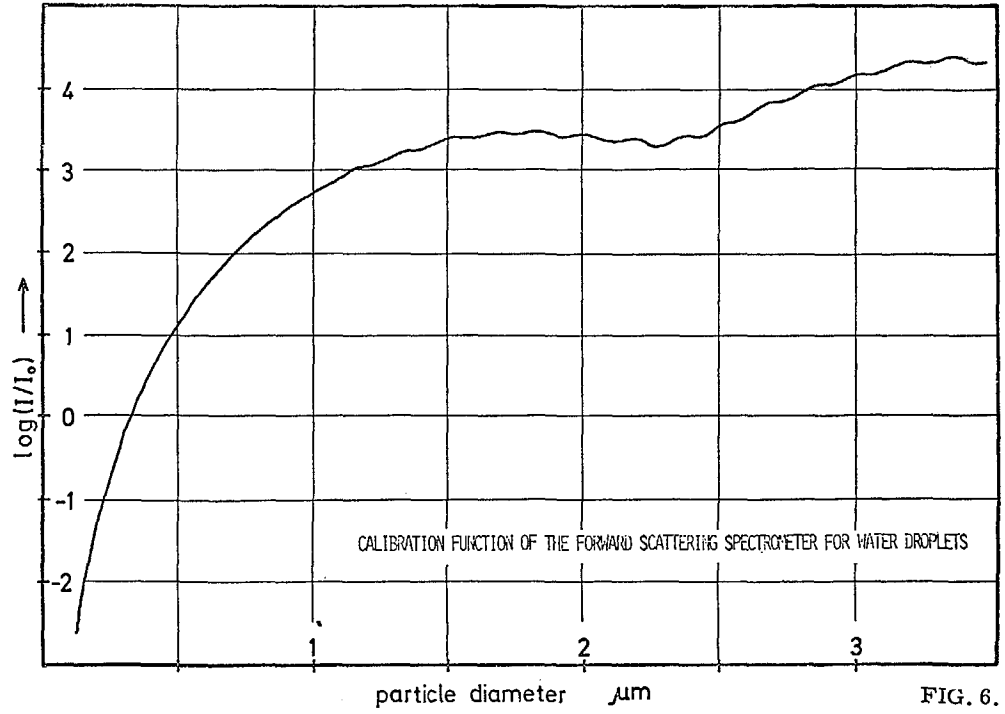

FIG. 6.

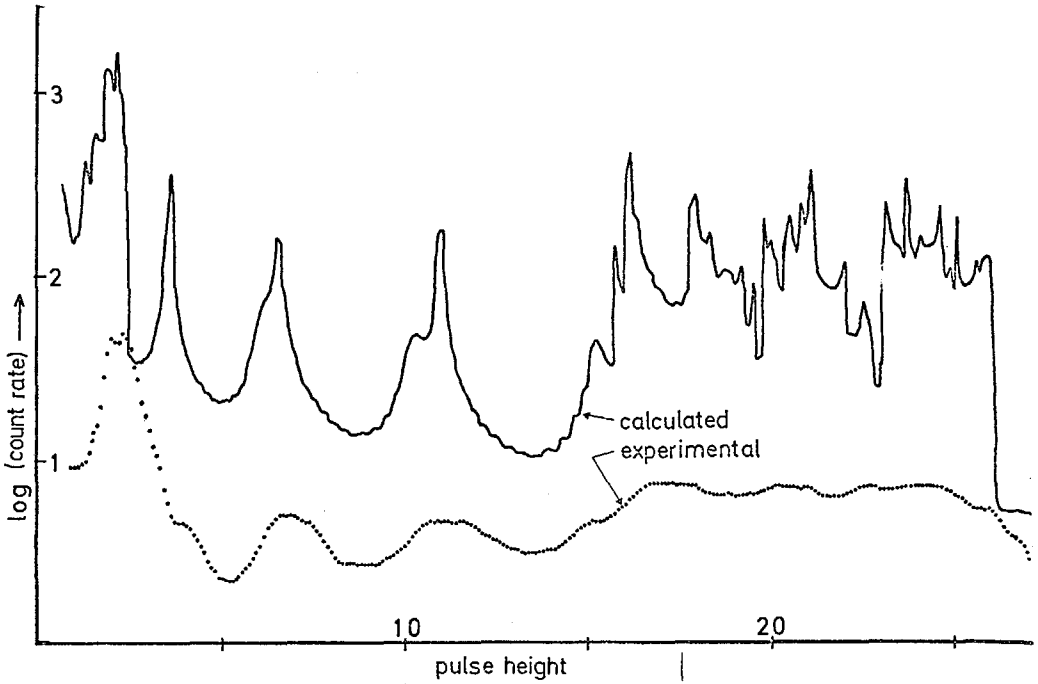

FIG. 7. CALCULATED AND MEASURED PULSE HEIGHT SPECTRA

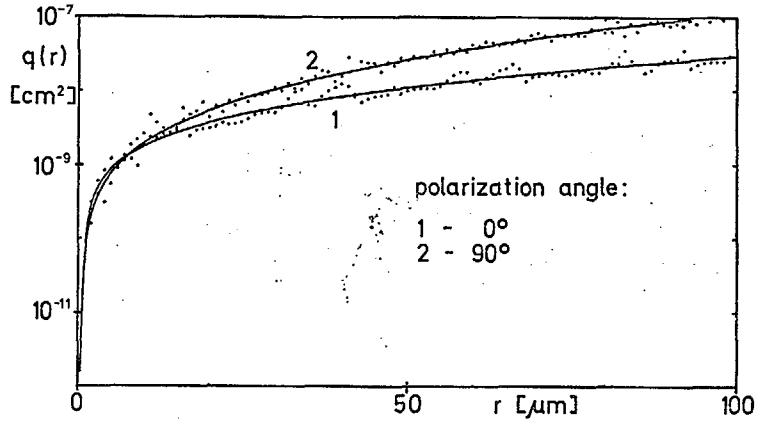

FIG. 9. CALIBRATION FUNCTIONS OF THE IN SITU SPECTROMETER

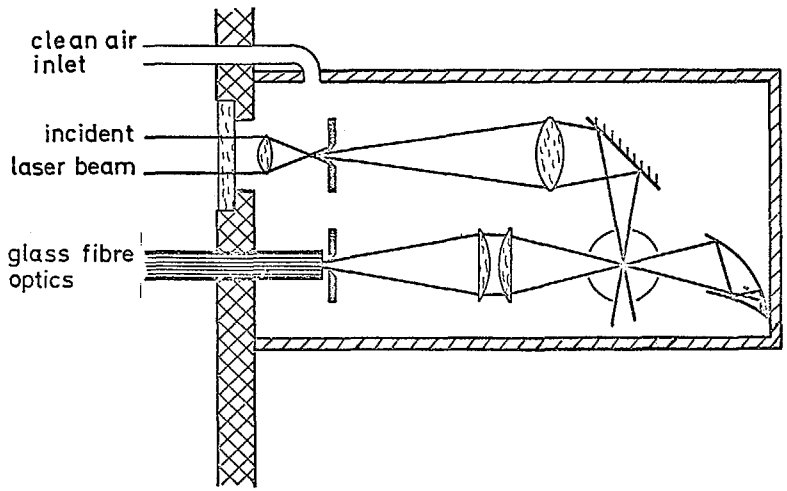

FIG. 8. OPTICAL SETUP OF THE IN SITU SPECTROMETER (SCHEMATIC)

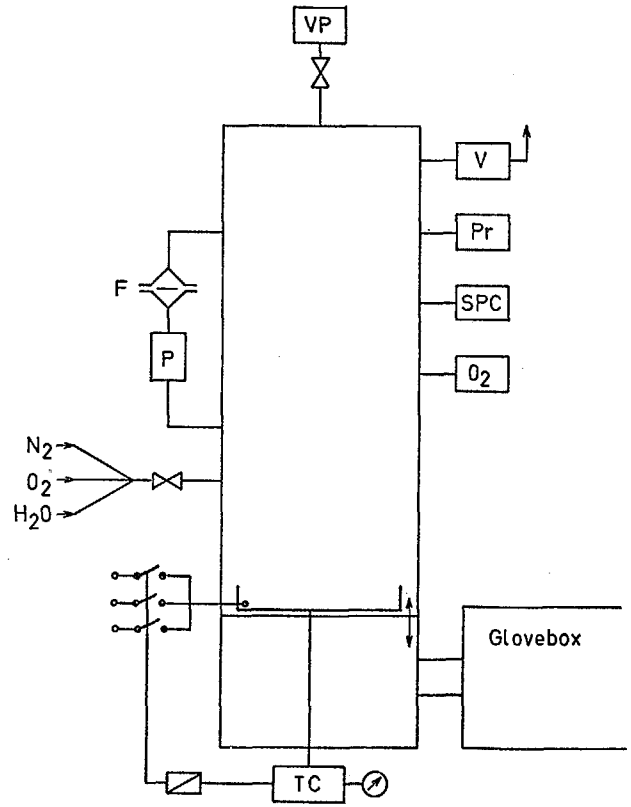

FIG. 10.

VP Vacuumpump
F Filter
P Pump
TC Temperature Control
V Valve
Pr Pressure Meter
O_2 Oxigenmeter
SPC Scintilation particle counter

Diagram of NABRAUS Test Facility

O_2-Concentration [%]	Burning Area [cm^2]	Burning Time [min]	Airborn Sodium [g]	Aerosol Formation Rate $\left[\frac{g \cdot Na}{cm^2 min}\right]$	$\left[\frac{kg \cdot Na}{m^2 \cdot h}\right]$
0.8	3080	60	464	0.0025	1.5
2	392	62	107	0.004	2.4
10	864	6	135	0.014	8.4
14	935	4	149	0.036	22
21	758	6	135	0.029	18
21	4770	14	1194	0.018	11
43	2110	8	800	0.048	29

FIG. 11. AEROSOL FORMATION RATES

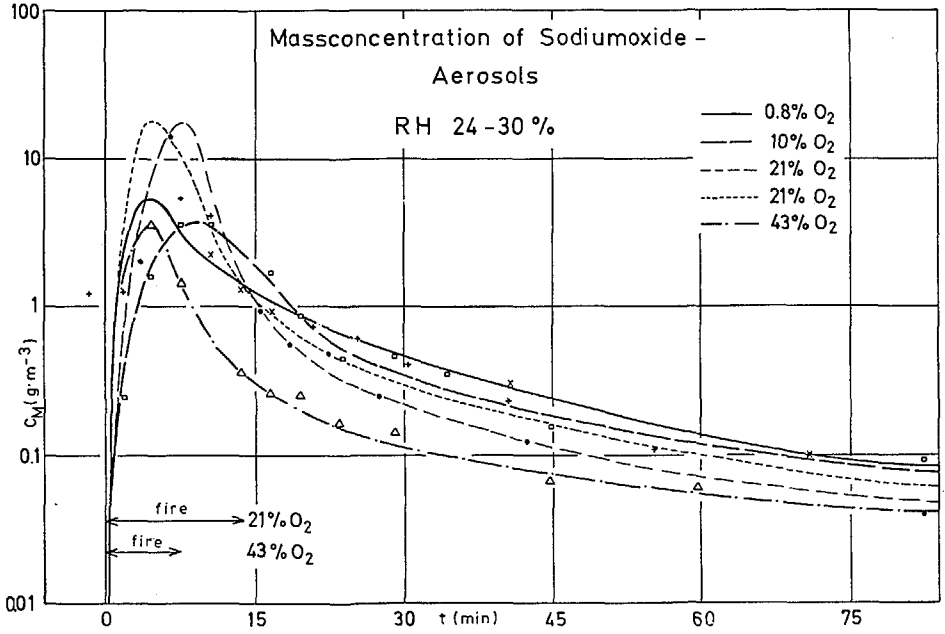

FIG. 12.

$[O_2]$ [%]	Cs - Content of Sodium Pool [PPM]	Maximum Aerosol - Concentration [MG/M^3]	Maximum Cs - Content of Aerosols [PPM]	MG CS/M^3	Cs - Content of Residue in Pool [PPM]
0	100	4040	1700	-	14
1	100	3940	1300	4,5	14
11	100	7600	480	3,6	
21	100	21400	200	4,2	37
22	100	11700	300	3,5	
21	200	11000	310	3,3	50
21	500	18000	1500		58

FIG. 13. Cesium Content of Aerosols above Contaminated Sodium Pools

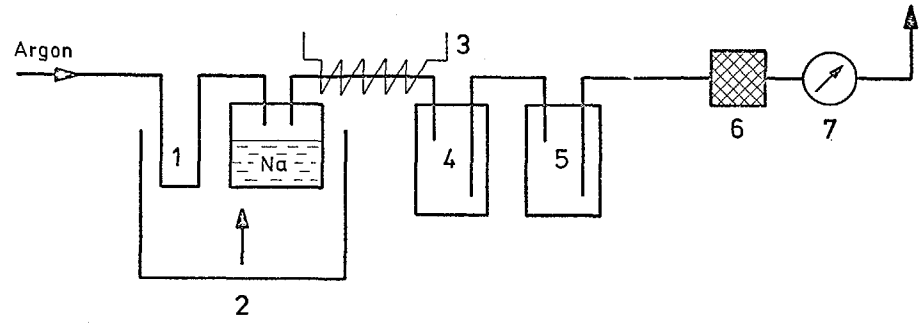

1 Preheater
2 Furnace
3 Heated Pipe
4,5 Cold Trap
6 Filter
7 Gasmeter

FIG. 14. Diagram of Experimental Facility

Experiment Nr.	Na g	UO_2 g	Temp. °C	Argon Flowrate l/min	Na trapped g	U trapped µg	DF
1	100	8,48	890	-	40,0	1580	2000
2	100	8,68	890	-	23,9	1230	1400
3	100	0,76	890	0,6	45,0	394	1100
4	100	0,84	500	17,0	12,3	42	2100
5	100	0,72	500	10,0	2,0	5	2470
6	100	0,95	500	1,0	0,9	4	1750
7	100	10,25	500	10,0	2,8	104	2450

FIG. 15. Release of Uranium from a Sodium Pool Contaminated with UO_2 - Particles

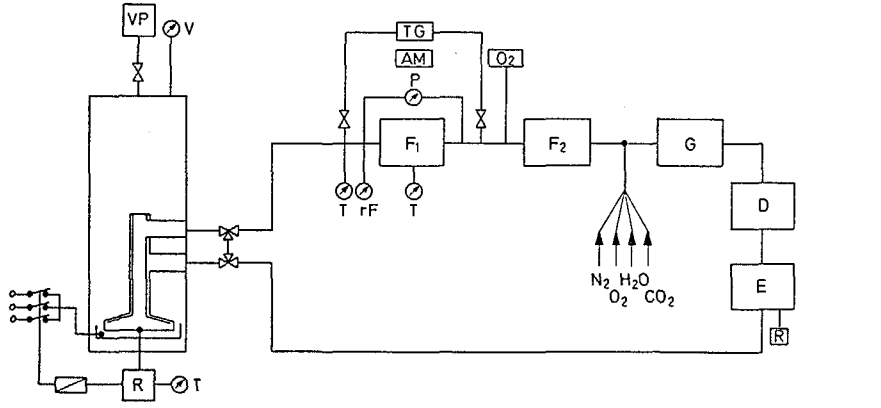

VP - Vacuumpump
F_1 - Test Filter
F_2 - Safety Filter
G - Blower
D - Flowmeter
E - Gasheater
R - Heatcontrol
V - Vacuummeter
T - Temperaturemeter
rF - Humiditymeter
P - Pressuremeter
O_2 - Oxygenmeter
AM - Aerosol-Massconc.-meter
TG - Particle-Size-Analyzer

FIG. 16. Diagram of the Filterloop

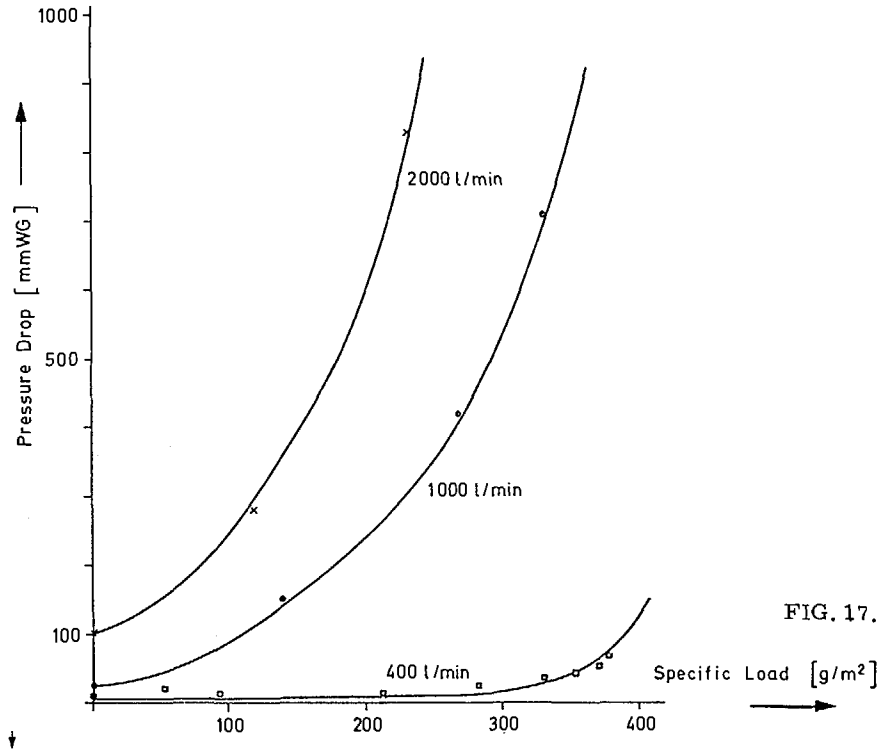

FIG. 17.

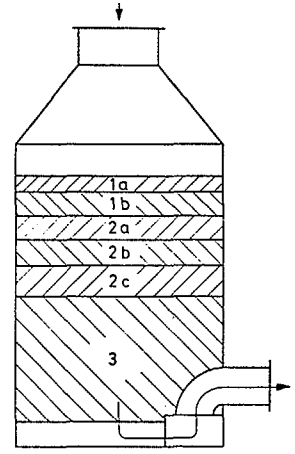

Packing I			400 l/min	1000 l/min	1500 l/min	2000 l/min
1a, 1b	150 kg 2/5	p	$6,4 \cdot 10^{-5}$	$1,4 \cdot 10^{-3}$	$1,2 \cdot 10^{-4}$	$3,2 \cdot 10^{-5}$
2a	50 kg 0,6/2					
2b	200 kg 0/0,6/0,6/2 1 : 3					
2c	-	B_S [g/m²]	446	465	-	352
3	200 kg 2/5					
Packing II			**400 l/min**	**550 l/min**	**775 l/min**	**1000 l/min**
1a	100 kg 2/5/5/11 1 : 3	p	$\approx 1,5 \cdot 10^{-5}$	$7,2 \cdot 10^{-5}$	$8,5 \cdot 10^{-5}$	$7,1 \cdot 10^{-5}$
1b	150 kg 2/5					
2a	50 kg 0,6/2					
2b	200 kg 0/0,6/0,6/2 1 : 3	B_S [g/m²]	443	396	660	600
2c	50 kg 0/0,6					
3	200 kg 2/5					

FIG. 18. Experimental Results for two Packings of Basalt Sand-Layers.